Hindawi
Shock and Vibration
Volume 2020, Article ID 6639372, 19 pages
https://doi.org/10.1155/2020/6639372

Research Article

Dynamic Analysis of High-Speed Helical Gear Transmission in Pure Electric Vehicle Gearbox

Yanchao Zhang,[1] **Jinfu Du**,[2] **Jin Mao**,[1] **and Min Xu**[3]

[1]*School of Mechanical and Precision Instrument Engineering, Xi'an University of Technology, Xi'an 710048, China*
[2]*Key Laboratory of Shaanxi Province for Development and Application of New Transportation Energy, Chang'an University, Xi'an 710064, China*
[3]*AECC Xi'an Engine Control Technology Co., Ltd., Xi'an 710077, China*

Correspondence should be addressed to Jinfu Du; dujinfu@xaut.edu.cn

Received 13 October 2020; Revised 19 November 2020; Accepted 24 November 2020; Published 7 December 2020

Academic Editor: Grzegorz Zywica

This study is to systematically analyze the influences of time-varying meshing stiffness (TVMS) and meshing impact on the dynamic characteristics of high-speed gear transmission in the two-stage pure electric vehicle (PEV) gearbox, as well as the effect of tooth surface modification on the vibration control. First, the dynamic model was established, and the TVMS and meshing impact were calculated. Then, the vibration characteristics of single-stage and two-stage helical gear transmission were analyzed under three different excitation conditions, excitation of TVMS, excitation of meshing impact, and excitation of both. The results show that the effect of rotating speed on the system vibration is not significant outside the resonant region under the excitation of TVMS, while the effect of meshing impact becomes the main exciting component with the increasing rotating speed. The vibrations of the two gear pairs interact with each other; the vibration frequency of one gear pair contains both its meshing frequency and the coupling frequency of the other gear pair. Tooth surface modification in the input-stage gear pair can reduce the vibration of both the input- and the output-stage obviously; that is, more attention should be paid to the input-stage gear pair in the modification design of PEV gearbox.

1. Introduction

With the aggravation of the energy and environment issue, the PEVs have shown a broad application prospect and achieved rapid development because of the advantages in energy conservation and environmental protection, as well as the performance and the potential for intelligent driving [1–3]. In the PEV power transmission system, the combination of electric motor and two-stage gearbox is widely used [4, 5], such as in Tesla Model S and NIO ES8. For increasing the power density ratio, the electric motor speed is relatively high. Thus, the gear pair of the input-stage often works in the high-speed off-resonance region. High rotating speed will necessarily bring a stern challenge to the dynamic performance of the gear transmission in PEV gearbox, which has a significant effect on vehicle reliability, stability, and vibration noise.

The dynamic characteristics of gear transmission system have always been a hot topic of scholars [6–8]. There are many excitation factors affecting the dynamic characteristics of gear transmissions. Among them, the meshing stiffness [9], errors [10], and the meshing impact [11] are the main internal excitations, and the frictional excitations along the line of action direction are the secondary excitations, when the aforementioned two kinds of excitations are minimized, the shuttling excitation along the axial direction may be dominant [12].

In early researches, TVMS was replaced by the mean meshing stiffness, while the accurate methods for calculating the TVMS have been proposed in recent years [13], and the influence of TVMS on the gear transmission has attracted wide attention. Saxena et al. calculated the gear meshing stiffness of misaligned shaft based on the potential energy method and studied the effect of misalignment and friction

on the cracked gear pair [14]. Later, a calculation method for meshing stiffness of helical gear considering the actual pitch deviation was proposed, and the influence mechanism of pitch deviation on the meshing stiffness and vibration noise of helical gears were analyzed by Yin et al. [15], and another accurate calculation method for the helical gear meshing stiffness was proposed by Tang et al. [16]. Han and Qi also proposed a TVMS of helical gears by slicing and discrete integral method, and the effects of gear tooth defects, such as cracks, pitting, spalling, and breakage, on TVMS were analyzed as well [17]. In a recent research, Sánchez et al. proposed the meshing stiffness equations including Hertzian effects for spur gears, as well as the approximate equations for the meshing stiffness and the load sharing ratio [18]. For the meshing impact, Chen et al. calculated the impact force of the sun gear in a planetary gear system under different loads, and the meshing stiffness and the dynamic transmission error of integrated planetary gear were investigated when the planetary gear meshed with the sun or ring gear [19]. In Wang's work, a dynamic model of herringbone gear including TVMS, meshing impact, and tooth surface friction was established and the vibration characteristics of the system were analyzed [20]. Zhou and Chen also proposed a meshing impact calculation method considering tooth surface friction [21].

Most of the above studies, however, are about the medium and low rotating speed conditions for single-stage gear transmission. On the one hand, as mentioned above, the input rotating speed of most of the gear transmissions in PEV field has reached more than 10000 rpm. The meshing impact has become a non-negligible internal excitation factor. On the other hand, the effects of excitation transfer and superposition between multistage gear pairs on the dynamic performance of the overall system are not negligible.

This paper focuses on finding out the effects of TVMS and meshing impact on the dynamic characteristics of high-speed helical gear transmissions in PEV gearbox, as well as the effect of tooth surface modification on the vibration control. A two-stage high-speed helical gear transmission system in a PEV reducer is taken as the research object in this study. First, the bending-torsion-axis dynamic model is established. Next, the TVMS, the impact time, and the amplitude of the impact force are calculated. Afterward, the dynamic characteristics of the single-stage and two-stage helical gear systems are analyzed under three kinds of excitation conditions, and the dynamic characteristics of the single-stage are compared to the two-stage gear systems as well. Finally, the effects of two modification schemes on the dynamic characteristics are studied, and some concluding remarks regarding this research are provided.

2. Dynamics Model

The 3D model and basic parameters of the two-stage high-speed helical gear transmission in the PEV reducer are shown in Figure 1 and Table 1, respectively.

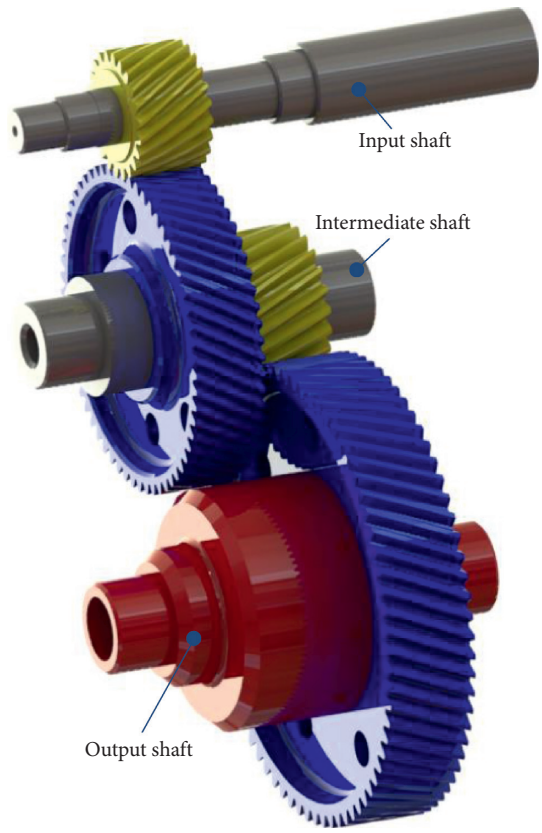

Figure 1: The two-stage high-speed helical gear transmission in a PEV reducer.

Table 1: Basic parameters of the gear transmission.

Parameters	Input pair	Output pair
Number of teeth z	22/59	23/71
Hand of spiral	LH/RH	LH/RH
Normal modulus m_n/(mm)	2	2.4
Normal pressure angle α/(°)	18.5	
Helix angle β/(°)	32	25
Face width b/(mm)	33/31.5	40/38
Elastic modulus E/(GPa)	210	
Input torque T/(N · m)	50	
Angle of axis plane γ_a/(°)	37	
Damping ratio ξ	0.1	
Gear mass m/(kg)	$5.3\times10^{-2}/2.5\times10^{-1}$	$6.5\times10^{-2}/3.8\times10^{-1}$
Moment of inertia I/(kg · m^2)	$1.7\times10^{-5}/3.9\times10^{-4}$	$3.2\times10^{-5}/1.1\times10^{-3}$

In two-stage helical gear transmission, the angle of the two planes of action α_m can be calculated by equation (1) according to Figure 2:

$$\alpha_m = \pi - \left(\frac{\pi}{2} - \alpha_2\right) - \left[\left(\frac{\pi}{2} - \alpha_1\right) + \gamma_a\right] = 2\alpha - \gamma_a, \quad (1)$$

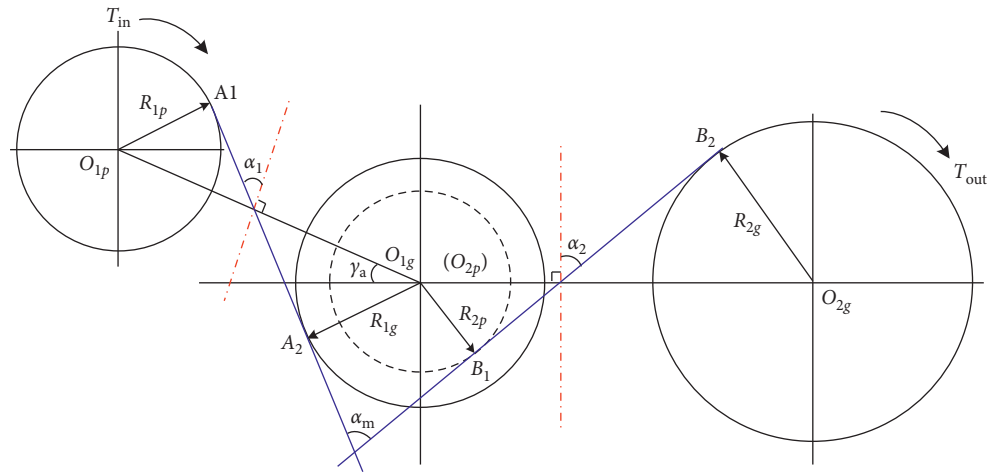

Figure 2: Angle of the two planes of action.

where T_{in}, T_{out} indicate the input and load torque, the tangents A_1A_2 and B_1B_2 represent the planes of action for each gear pair, the base radii of each gear are $R_{1p}, R_{1g}, R_{2p}, R_{2g}$, the working pressure angles are α_1 and α_2, and the angle of two axis planes is γ_a. For the two-stage gear transmission given in Table 1, the calculation result of α_m is 0°. That is, the two planes of action are parallel. Therefore, the following dynamic model is established by the lumped-mass method, as shown in Figure 3. $m_{1p}, m_{1g}, m_{2p}, m_{2g}$ and $I_{1p}, I_{1g}, I_{2p}, I_{2g}$are the mass and the inertia moment of the gears; the values of the equivalent support stiffness $k_{1py}, k_{1pz}, k_{12y}, k_{12z}, k_{2gy}, k_{2gz}$ and damping $c_{1py}, c_{1pz}, c_{12y}, c_{12z}, c_{2gy}, c_{2gz}$, as well as the torsional stiffness k_θ and dampingc_θ of the intermediate shaft, are given in Table 2.

Then, the differential equations of this helical gear transmission system are derived:

$$\begin{cases} m_{1p}\ddot{y}_{1p} + c_{1py}\dot{y}_{1p} + k_{1py}y_{1p} = -F_{y1}, \\ m_{1p}\ddot{z}_{1p} + c_{1pz}\dot{z}_{1p} + k_{1pz}y_{1p} = -F_{z1}, \\ I_{1p}\ddot{\theta}_{1p} = -F_{y1}R_{1p} + T_{in} - F_{s1}R_{1p}, \\ (m_{1g} + m_{2p})\ddot{y}_{12} + c_{12y}\dot{y}_{12} + k_{12y}y_{12} = F_{y1} - F_{y2}, \\ (m_{1g} + m_{2p})\ddot{z}_{12} + c_{12z}\dot{z}_{12} + k_{12z}z_{12} = F_{z1} - F_{z2}, \\ I_{1g}\ddot{\theta}_{1g2p} + c_\theta(\dot{\theta}_{1g} - \dot{\theta}_{2p}) + k_\theta(\theta_{1g} - \theta_{2p}) = (F_{y1} + F_{s1})R_{1g}, \\ I_{2p}\ddot{\theta}_{1g2p} + c_\theta(\dot{\theta}_{2p} - \dot{\theta}_{1g}) + k_\theta(\theta_{2p} - \theta_{1g}) = (F_{y2} + F_{s2})R_{2p}, \\ m_{2g}\ddot{y}_{2g} + c_{2gy}\dot{y}_{2g} + k_{2gy}y_{2g} = F_{y2}, \\ m_{2g}\ddot{z}_{2g} + c_{2gz}z_{2g} + k_{2gz}z_{2g} = F_{z2}, \\ I_{2g}\ddot{\theta}_{2g} = F_{y2}R_{2g} - T_{out} + F_{s2}R_{2g}, \end{cases} \tag{2}$$

where y_{1p}, z_{1p} indicate the vibration displacements of the input shaft, the vibration displacements of intermediate and output shaft are y_{12}, z_{12} and y_{2g}, z_{2g}, the torsional displacements of the gears are θ_{1p}, θ_{1g}, θ_{2p}, θ_{2g}, the relative angle of gear 1 and pinion 2 is θ_{1g2p}, and the meshing impacts of two gear pairs are represented by F_{s1}, F_{s2}. The displacement matrix of this system can be expressed as

$$\{\delta\} = \{y_{1p}\ \ z_{1p}\ \ \theta_{1p}\ \ y_{12}\ \ z_{12}\ \ \theta_{1g}\ \ \theta_{2p}\ \ y_{2g}\ \ z_{2g}\ \ \theta_{2g}\}^T. \tag{3}$$

To compare the dynamic characteristics of the single-stage gear system with the two-stage gear system, the differential equations of the input gear pair are as follows:

$$\begin{cases} m_{1p}\ddot{y}_{1p} + c_{1py}\dot{y}_{1p} + k_{1py}y_{1p} = -F_{y1}, \\ m_{1p}\ddot{z}_{1p} + c_{1pz}\dot{z}_{1p} + k_{1pz}y_{1p} = -F_{z1}, \\ I_{1p}\ddot{\theta}_{1p} = -F_{y1}R_{1p} + T_{in} - F_{s1}R_{1p}, \\ m_{1g}\ddot{y}_{1g} + c_{12y}\dot{y}_2 + k_{12y}y_2 = F_{y1}, \\ m_{1g}\ddot{z}_{1g} + c_{12z}z_2 + k_{12z}z_2 = F_{z1}, \\ I_{1g}\ddot{\theta}_{1g} = F_{y12}R_{b2} - T_{1g} + F_{s1}R_{1g}. \end{cases} \tag{4}$$

The tangential and axial dynamic meshing forces of the system are expressed in

$$\begin{cases} F_{yi} = \cos\beta_i\{c_{mi}[\cos\beta_i(\dot{y}_{ip} - \dot{y}_{ig} + R_{ip}\dot{\theta}_{ip} - R_{ig}\dot{\theta}_{ig}) + \sin\beta_i(\dot{z}_{ip} - \dot{z}_{ig})] + k_i(t)[\cos\beta_i(y_{ip} - y_{ig} + R_{ip}\theta_{ip} - R_{ig}\theta_{ig}) + \sin\beta(z_{ip} - z_{ig})]\}, \\ F_{zi} = \sin\beta_i\{c_{mi}[\cos\beta_i(\dot{y}_{ip} - \dot{y}_{ig} + R_{ip}\dot{\theta}_{ip} - R_{ig}\dot{\theta}_{ig}) + \sin\beta_i(\dot{z}_{ip} - \dot{z}_{ig})] + k_i(t)[\cos\beta_i(y_{ip} - y_{ig} + R_{ip}\theta_{ip} - R_{ig}\theta_{ig}) + \sin\beta_i(z_{ip} - z_{ig})]\}, \end{cases} \tag{5}$$

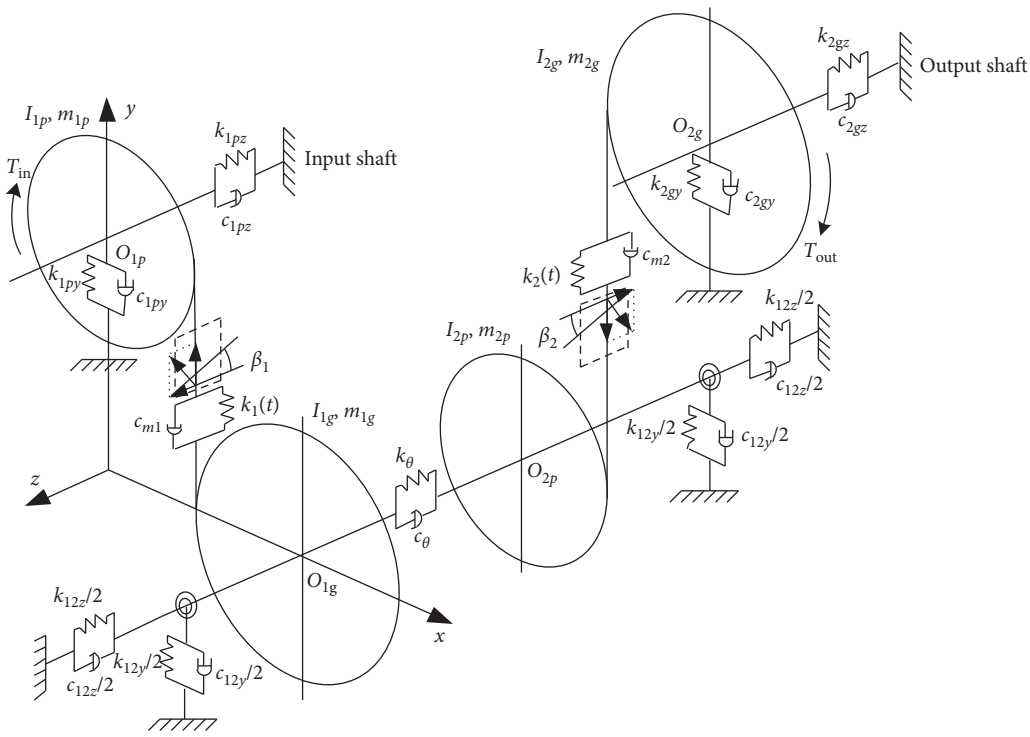

Figure 3: Dynamics model of the helical gear transmission system.

Table 2: Equivalent stiffness and damping.

Parameters	Input shaft	Intermediate shaft	Output shaft
Equivalent radial stiffness k_y/(N/m)	1.9×10^8	8.3×10^8	8.3×10^8
Equivalent axial stiffness k_z/(N/m)	8.3×10^6	1.2×10^7	1.2×10^7
Equivalent radial damping c_y/(N · s/m)	6.3×10^2	3.3×10^3	3.6×10^3
Equivalent axial damping c_z/(N · s/m)	1.3×10^2	3.9×10^2	4.3×10^2
Torsional stiffness k_θ/(N · m/rad)		8.5×10^4	
Torsional damping c_θ/(N · s/m)		2.4	

where $k_i(t)$ $(i = 1, 2)$ indicates the TVMS; the helix angles β_i $(i = 1, 2)$ and pressure angle α are given in Table 1.

The formula for calculating the meshing damping c_{mi} $(i = 1, 2)$ is shown in

$$c_{mi} = 2\xi\sqrt{\frac{k_i I_{ip} I_{ig}}{I_{ip}R_{ig} + I_{ig}R_{ip}}}, \tag{6}$$

where ξ is the damping ratio.

To eliminate the influence of the angular displacement of the gear rigid body on the subsequent analysis, the relative angular displacement q is introduced to convert the angular displacement into linear displacement, as shown in

$$\begin{cases} q_1 = R_{1p}\theta_{1p} - R_{1g}\theta_{1g}, \\ q_2 = R_{2p}\theta_{2p} - R_{2g}\theta_{2g}. \end{cases} \tag{7}$$

The subscripts 1 and 2 represent the input and output gear pair, respectively. Substituting equation (7) into equations (4) or (3),

$$\begin{cases} m_1\ddot{q}_1 + F_{y1} = \dfrac{T_{in}}{R_{1p}} - F_{s1}, \\ m_2\ddot{q}_2 + F_{y2} = \dfrac{T_{out}}{R_{2p}} - F_{s2}, \end{cases} \tag{8}$$

where m_1 and m_2 are the equivalent torsional qualities of the gear pairs:

$$\begin{cases} m_1 = \dfrac{I_{1p}I_{1g}}{I_{1p}R_{1g}^2 + I_{1g}R_{1p}^2}, \\ m_2 = \dfrac{I_{2p}I_{2g}}{I_{2p}R_{2g}^2 + I_{2g}R_{2p}^2}. \end{cases} \tag{9}$$

3. Calculation of the TVMS

The TVMS is calculated based on the improved loaded tooth contact analysis (LTCA) method [22]. This LTCA method

combines the gear geometry analysis with the mechanical analysis organically, and many factors such as actual coincidence degree and error are considered comprehensively [23], and the tooth surface load distribution P as well as the loaded transmission error (LTE) Z under the current contact position load can be obtained. The LTE is then converted into the meshing normal deformation δ_n according to

$$\delta_n = \frac{Z \cdot m_n z_2 \cos \alpha_t}{2 \cos^2 \beta}, \tag{10}$$

where m_n, z_2, and α_t represent the normal modulus, the number of driven teeth, and the end pressure angle, respectively.

The TVMS $k(t)$ is then obtained:

$$k(t) = \frac{P}{\delta_n}. \tag{11}$$

The LTE of the gear pair is mainly caused by the geometric transmission error (TE), the gear tooth bending deformation, and tooth surface contact deformation. The TE is determined by tooth surface design and machining. When the material, the geometric parameters, and the meshing position are confirmed, the tooth bending deformation and the contact deformation are determined by the load, which can be obtained according to the following equation [24]:

$$\begin{cases} \delta_1(P) = c_1, \\ \delta_2(P) = c_2 P, \\ \delta_3(P) = c_3 \sqrt[3]{P^2}, \end{cases} \tag{12}$$

where c_1, c_2, c_3 represent the underdetermined coefficients, while $\delta_1, \delta_2, \delta_3$ represent the geometric transmission error, the tooth bending deformation, and the contact deformation.

The meshing period is divided into n parts, and $Z_k(P)$ represents the deformation of the k-th ($k = 1, 2, \ldots, n+1$) meshing point under the nominal load P, which can be obtained by the gear LTCA program.

Thus, the load deformation of the k-th meshing position under the nominal load can be expressed as

$$Z_k(P) = c_1 + c_2 P + c_3 \sqrt[3]{P^2}. \tag{13}$$

The LTE of meshing positions under a given load can be obtained by LTCA, and the meshing stiffness of each point is calculated by equations (10) and (11). By the curve fitting method, the TVMS function is then derived under a certain load.

The LTEs of a meshing point under three different loads can be obtained by the same method. And then the coefficients c_1, c_2, c_3 can be determined; the relationship between load and deformation of the gear pair under different loads can be obtained. The meshing stiffness of a certain meshing point under any load can then be obtained. Finally, the TVMS can be obtained under any load conditions by computations on each meshing point in the whole meshing period.

According to the previous method, the TVMS curve of the input-stage and output-stage gear pairs of the PEV reducer under torque $100\,\mathrm{N \cdot m}$ is calculated and shown in Figure 4:

4. Calculation and Analysis of the Meshing Impact

The meshing points of the ideal gear pair (without error deformation) are on the theoretical meshing line. Due to the meshing synthesis pitch error caused by the gear machining error, the installation error, and the deformation of the gear, the base pitch of two gears is no longer equal, so the meshing point of the gear pair deviates from the theoretical meshing line at the meshing-in and meshing-out position. Thus, the gear transmission ratio and meshing force change abruptly, which leads to vibration and noise.

The formation mechanisms of the above two meshing impacts are the same, but the effect of the meshing-in impact is more significant than the meshing-out impact. Thus, only the meshing-in impact is considered in this study. The schematic of the meshing-in impact is shown in Figure 5.

In Figure 5, the points O_p, O_g indicate the centre of the pinion and the wheel, the pitch point is A, the point D is the starting position of the out-of-line meshing, while point E is the starting position of normal meshing, the inversion point of point E is E', and the combined deformation amount of the meshing teeth δ can be obtained by LTCA method. According to the geometric relationship of $\Delta O_p D O_g$ and $\Delta A D O_g$, the following equations can be obtained:

$$\varphi = \frac{\delta}{r_{\mathrm{ag}}}, \tag{14}$$

$$\angle AEO_g = \arcsin \frac{r_g \sin((\pi/2) + \alpha)}{r_{ag}}, \tag{15}$$

$$\gamma_g = \left(\frac{\pi}{2}\right) - \alpha - \angle AEO_g, \tag{16}$$

$$\angle AO_g D = \gamma_g + \varphi + \Delta\varphi_g, \tag{17}$$

$$r_{O_p D} = \sqrt{a_c^2 + r_{ag}^2 - 2 a_c r_{ag} \cos\left(\angle AO_g D\right)}, \tag{18}$$

$$r_{O_p E} = \sqrt{a_c^2 + r_{ag}^2 - 2 a_c r_{ag} \cos \gamma_g}, \tag{19}$$

$$\angle AO_p D - \Delta\varphi_p - \angle AO_p E = \angle DO_p E', \tag{20}$$

where r_{ap}, r_{ag}, R_p, R_g, r_p, r_g are the tooth tip circle radius, base circle radius, and pitch circle radius, and the centre distance is a_c.

Substituting equations (14)–(19) into equation (20), $\Delta\varphi_p$ can then be obtained, as well as the impact time Δt:

$$\Delta t = \frac{\Delta\varphi_p}{\omega_1}, \tag{21}$$

where ω_1 is the angular velocity of the pinion.

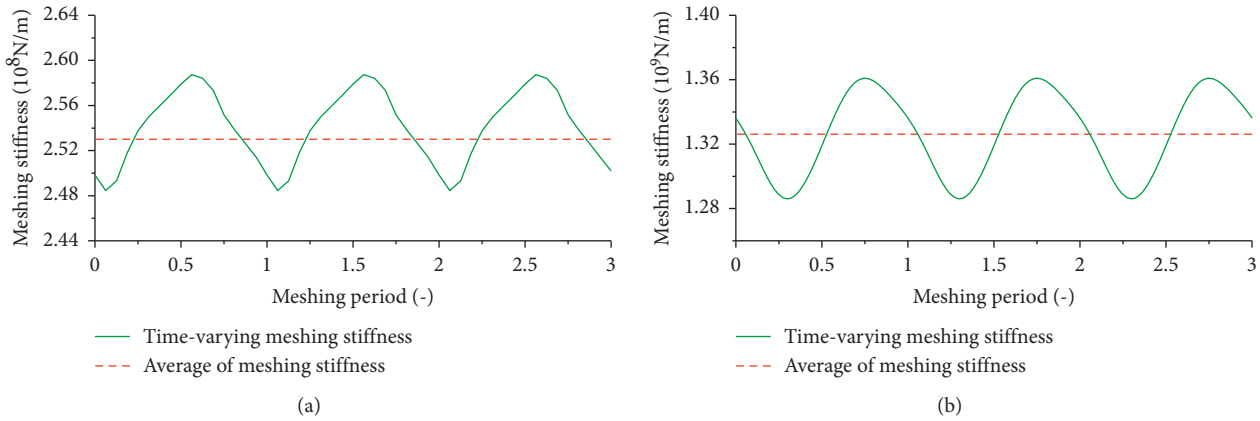

Figure 4: The TVMS curve: (a) input-stage; (b) output-stage.

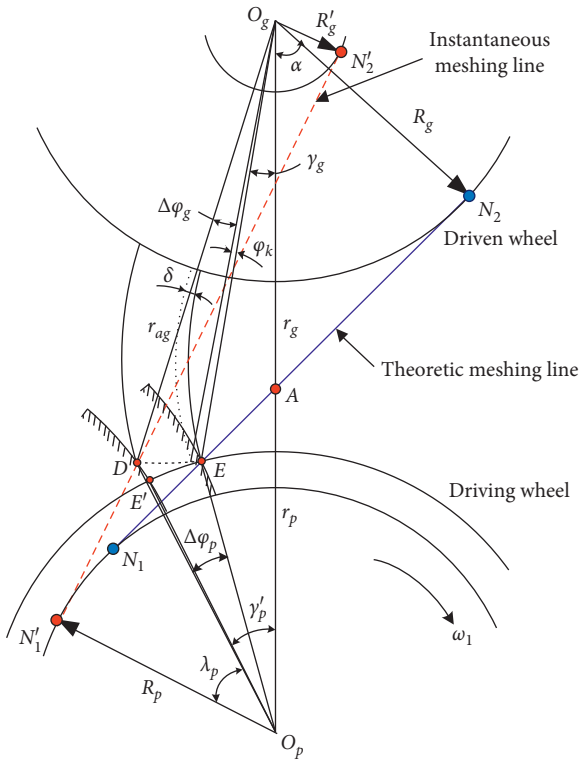

Figure 5: Schematic diagram of meshing-in impact.

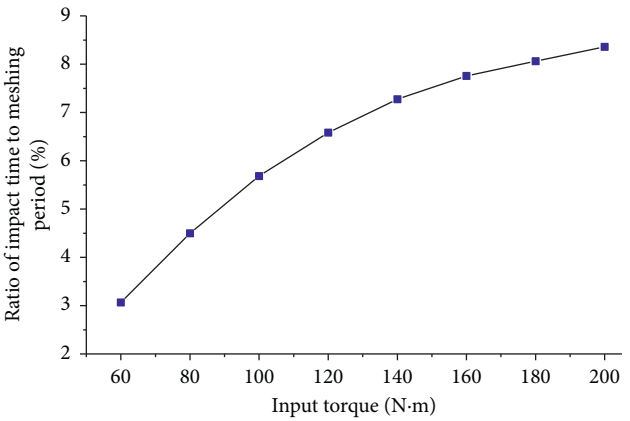

Figure 6: The change of meshing impact time with load.

According to the results of the above theoretical derivation, the meshing impact time is only related to the meshing teeth comprehensive deformation δ when the gear size parameters are determined. The load torque is an important factor affecting the δ. Figure 6 shows the change of the impact time under different loads.

It is seen from Figure 6 that the percentage of the meshing impact in the meshing period is within 3%–8.4%, and as the load torque increases, the percentage gradually levels off, because the increase of load torque will enlarge the contact area to increase the load-carrying capacity of the tooth surface.

According to the theory of impact dynamics, the amplitude of the impact force can be obtained by the following equation:

$$\begin{cases} F_s = v_s \sqrt{\dfrac{J_p J_g}{\left(J_p R_g'^2 + J_g R_p^2\right) q_s}}, \\ v_s = \dfrac{\omega_1 R_p (1+i)\left(\cos\alpha - \cos\left(\lambda_p + \gamma'_p\right)\right)}{i\cos\alpha}. \end{cases} \tag{22}$$

Here, v_s indicates the impact velocity of the point of meshing-in, and q_s is the single-tooth compliance of the point meshing-in, and the variables J_p, J_g, and i indicate the rotational inertia of driving and driven wheels and the gear transmission ratio. The driving wheel base radius is R_p, while the instantaneous base circle radius of the driven wheel is R'_g.

Since the impact time is relatively short, the meshing impact force is usually reduced to a sawtooth wave function. Based on the percentage of the meshing impact and the amplitude of the impact force obtained above, the meshing impact force curve is shown in Figure 7.

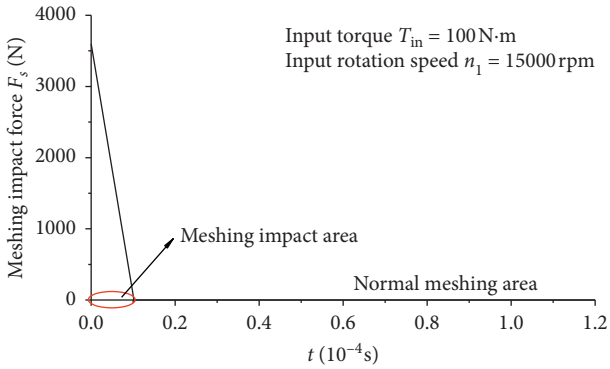

Figure 7: Meshing impact force curve.

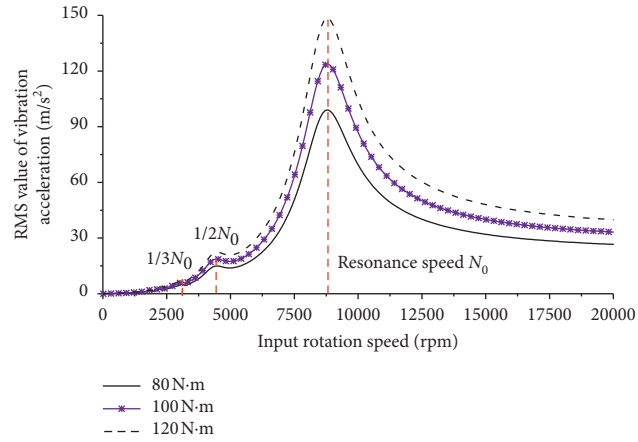

Figure 8: The vibration acceleration diagram of the single-stage gear system under excitation of TVMS.

5. Dynamic Analysis at High Speed

The vibration accelerations in all directions of the gear are synthesized as the relative vibration acceleration a in the line of action on the end face of the gear, which is regarded as the main index to measure the vibration of the system, as is shown in

$$a_i = \cos\beta_i\left(\ddot{y}_{ip} - \ddot{y}_{ig} + \ddot{q}_i\right) + \sin\beta_i\left(\ddot{z}_{ip} - \ddot{z}_{ig}\right). \quad (23)$$

Then, the root mean square (RMS) value can be calculated, and the vibration acceleration diagram can be obtained. The dynamic characteristics of the helical gear transmission system are then analyzed under three kinds of excitation conditions, excitation of TVMS, excitation of meshing impact, and excitation of both of them.

5.1. Excitation of TVMS. The TVMS curve obtained above is substituted into the dynamic equations, and the vibration responses of the single-stage gear system are obtained under the input torques of 80 N · m, 100 N · m, and 120 N · m. The vibration acceleration diagrams are shown in Figure 8.

As is shown in Figure 8, the 2nd- and 3rd-order superharmonic resonance occur when the rotating speed approaches 1/2 and 1/3 resonance speed N_0. The vibration increases with the increase of load torque. The RMS value of the vibration acceleration is not significantly increased with the increase of the rotating speed excluding the resonance peak; on the contrary, there is a slight downward trend after the resonance region. That is, the effect of speed increasing on the vibration characteristics is not significant under the excitation of TVMS when the speed is far away from the resonance speed. This is because the TVMS is a parameter excitation. The vibration of the system under parametric excitation is called parametric vibration. The system has no external force input except the driving force, so the system vibration is caused by the periodic change of the system internal parameters. As the rotating speed increases to the off-resonance zone, the frequency of parameter excitation gradually moves away from the system resonance frequency, so the influence of this parameter change on the system also decreases. Therefore, the system vibration does not increase significantly with the rotating speed increase under the excitation of TVMS in the off-resonance zone.

To analyze the dynamic characteristics of the two-stage helical gear transmission system, and compare the dynamic characteristic differences between the single-stage and two-stage helical gear transmission system, the vibration responses of the above two systems are analyzed under the excitation of TVMS at 3,000 rpm and 15,000 rpm, as is shown in Figures 9–14.

Figures 9 and 10 show the vibration responses of a single-stage helical gear transmission system at 3,000 rpm and 15,000 rpm. As can be seen, the phase diagram of the single-stage helical gear transmission system is a closed curve under the excitation of TVMS. And the Poincaré section is a single point. It is an obvious periodic appearance for the vibration response. And the system response frequency only has its meshing and multiplication frequency; the frequency component is relatively simple. Figures 11–14 show the vibration responses of the input-stage gear pair of the two-stage helical gear transmission system at 3,000 rpm and 15,000 rpm. f_{z1} represents the meshing frequency of the input gear pair, and f_{z2} represents the meshing frequency of the output gear pair. f_{z1} f_{z2} As can be seen from (b) and (d) in Figures 11–14, the phase diagram of the two-stage helical gear transmission system under the excitation of TVMS is a series of curves intersecting with each other, and the Poincaré section is a series of discrete points that can form a closed curve. Therefore, the vibration responses show distinct quasiperiodic characteristics. The nonperiodic vibration response of the two-stage helical gear transmission system is significantly enhanced, compared with the single-stage helical gear transmission system.

As can be seen from (c) in Figures 11–14, the frequency domain response component of the two-stage gear system becomes complicated. In addition to its own meshing frequency component, the vibration frequency of the input-stage gear pair also includes the meshing frequency of the output-stage gear pair and the frequencies of the overlapping and combination of the two meshing frequencies. This phenomenon also exists in the vibration frequency domain diagram of the output-stage gear pair. Since the input-stage gear pair is the power source of the output-stage gear pair, this phenomenon

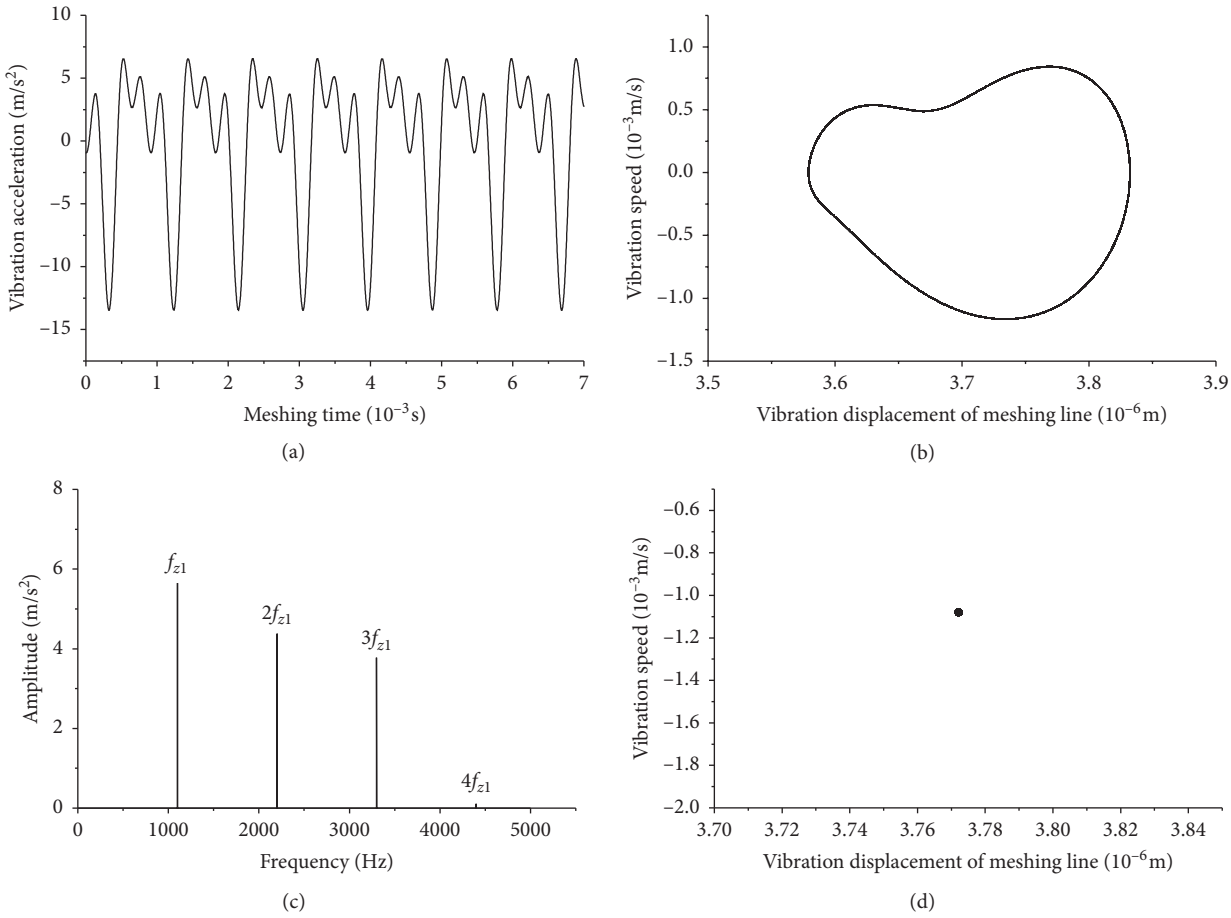

Figure 9: Vibration response of single-stage helical gear transmission system at 3,000 rpm: (a) time-domain diagram, (b) phase diagram, (c) frequency-domain diagram, and (d) Poincaré section.

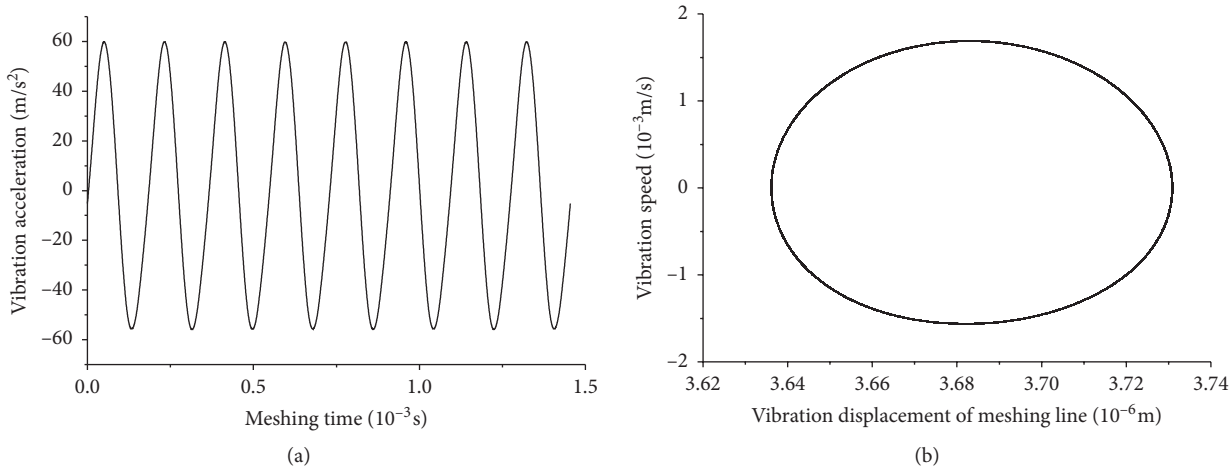

Figure 10: Continued.

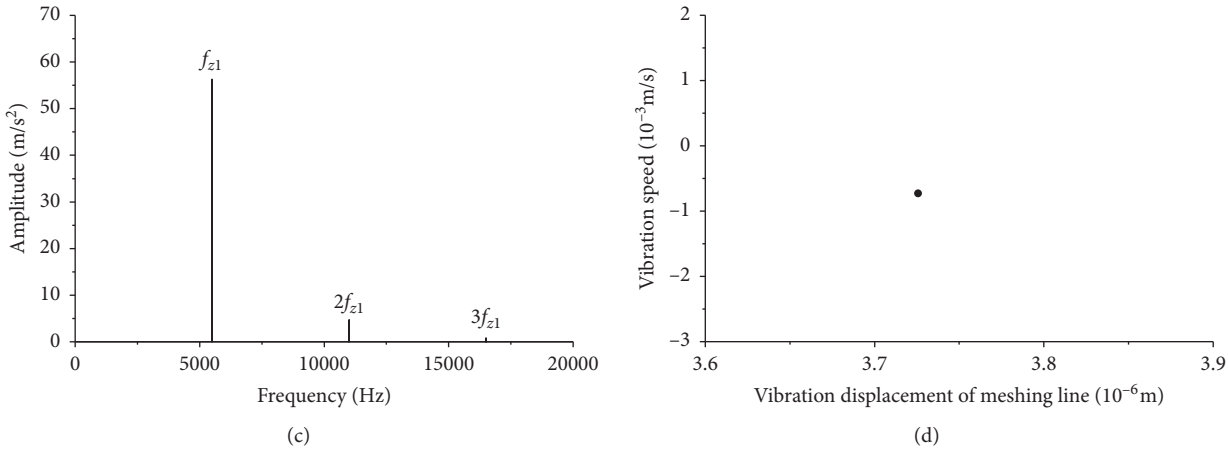

Figure 10: Vibration response of single-stage helical gear transmission system at 15,000 rpm: (a) time-domain diagram, (b) phase diagram, (c) frequency-domain diagram, and (d) Poincaré section.

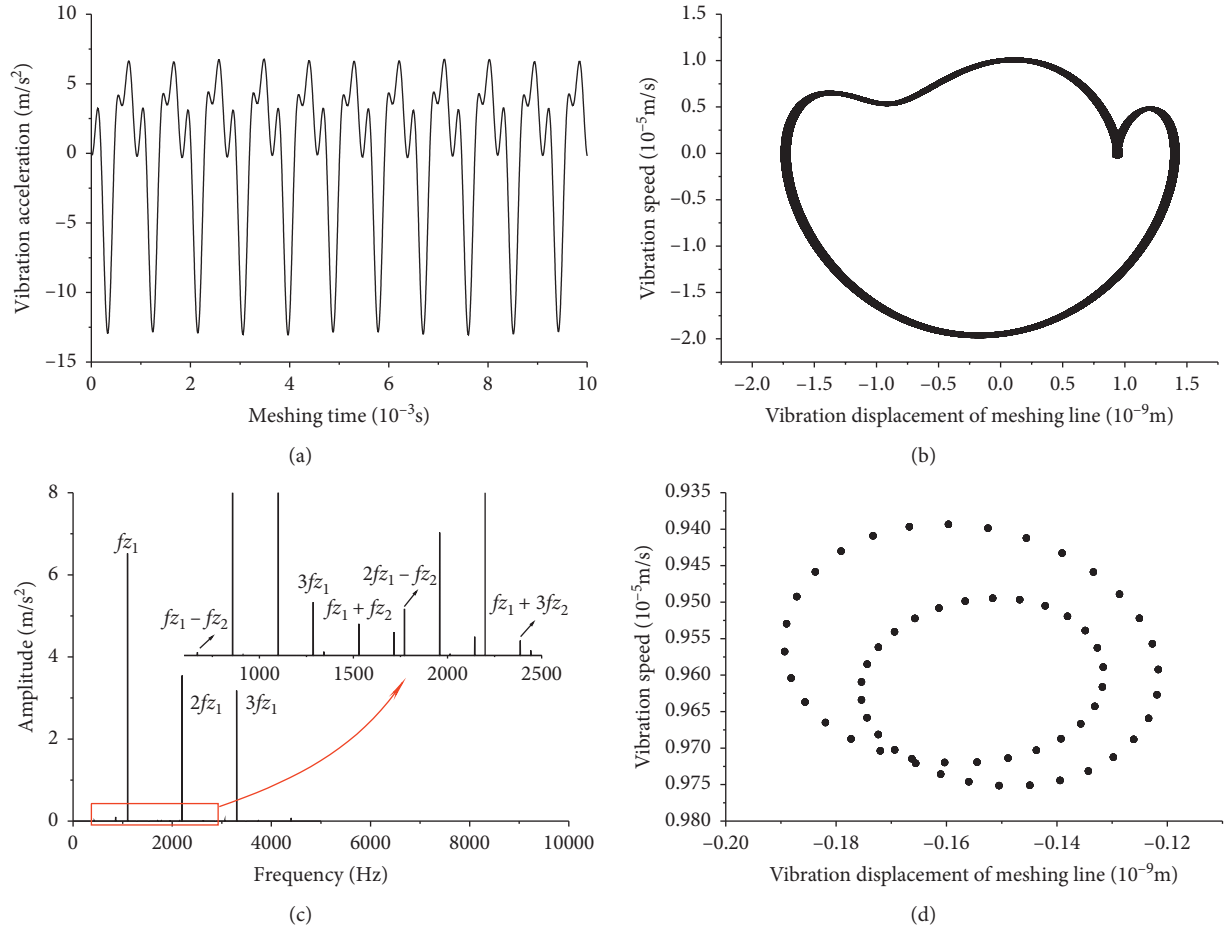

Figure 11: Vibration response of the input-stage gear pair of a two-stage helical gear transmission system at 3,000 rpm: (a) time-domain diagram, (b) phase diagram, (c) frequency-domain diagram, and (d) Poincaré section.

is more obvious in the output-stage gear pair, as shown in Figure 12(c); in the frequency response of the output-stage gear pair, the higher amplitudes are mostly related to the meshing frequency of the input-stage gear pair; however, the response frequency amplitude related to the meshing frequency of the output-stage gear pair is not that large.

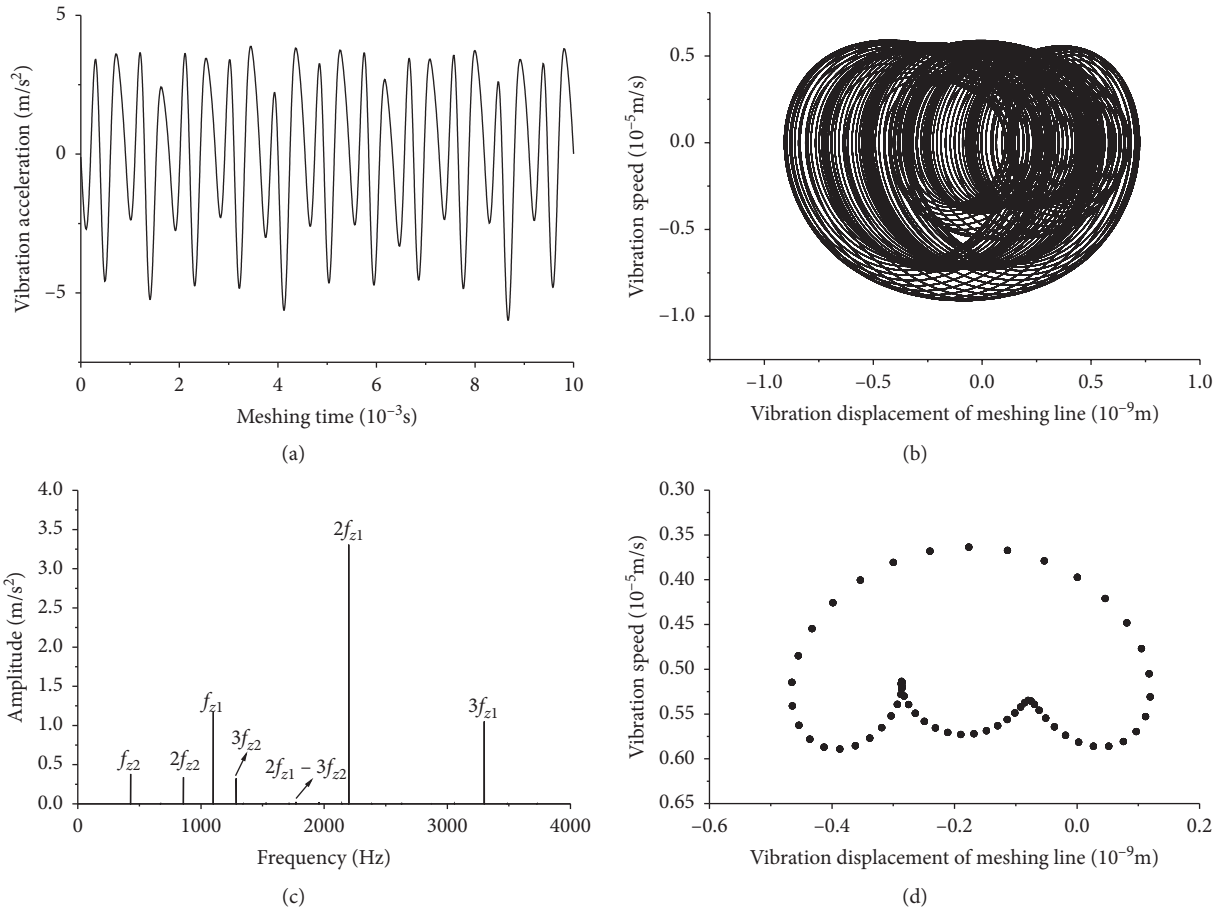

Figure 12: Vibration response of the output-stage gear pair of a two-stage helical gear transmission system at 3,000 rpm: (a) time-domain diagram, (b) phase diagram, (c) frequency-domain diagram, and (d) Poincaré section.

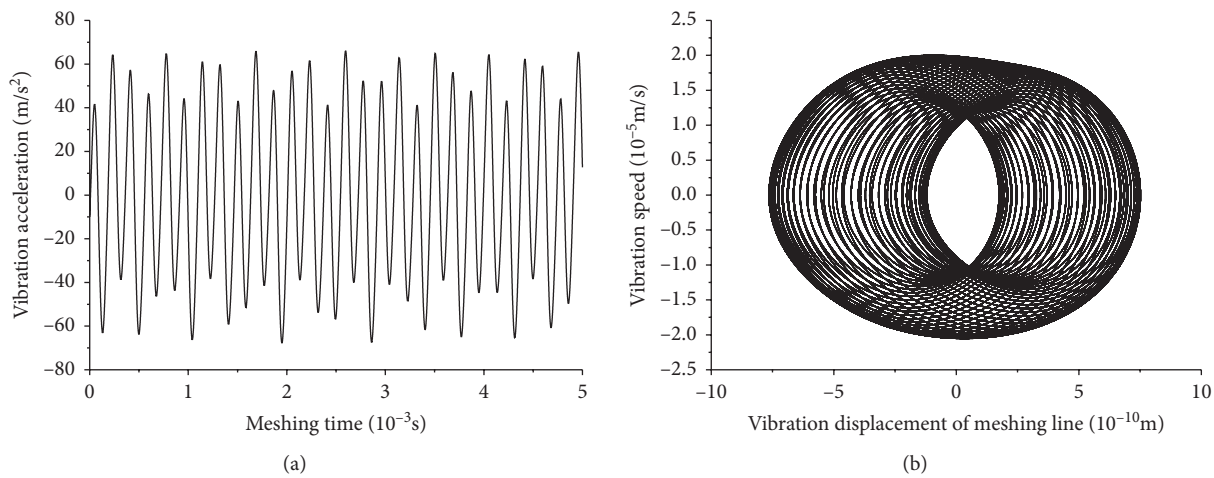

Figure 13: Continued.

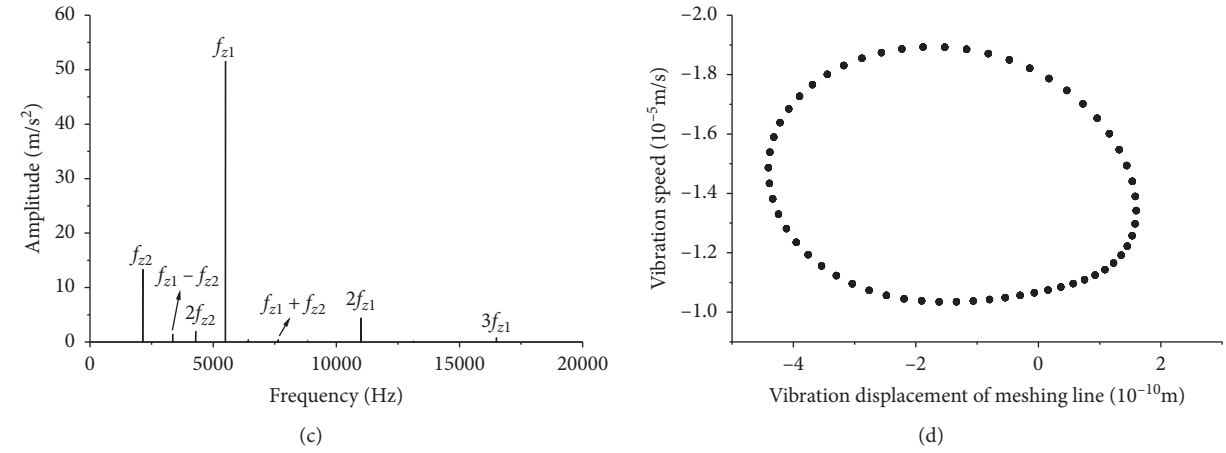

Figure 13: Vibration response of the input-stage gear pair of a two-stage helical gear transmission system at 15,000 rpm: (a) time-domain diagram, (b) phase diagram, (c) frequency-domain diagram, and (d) Poincaré section.

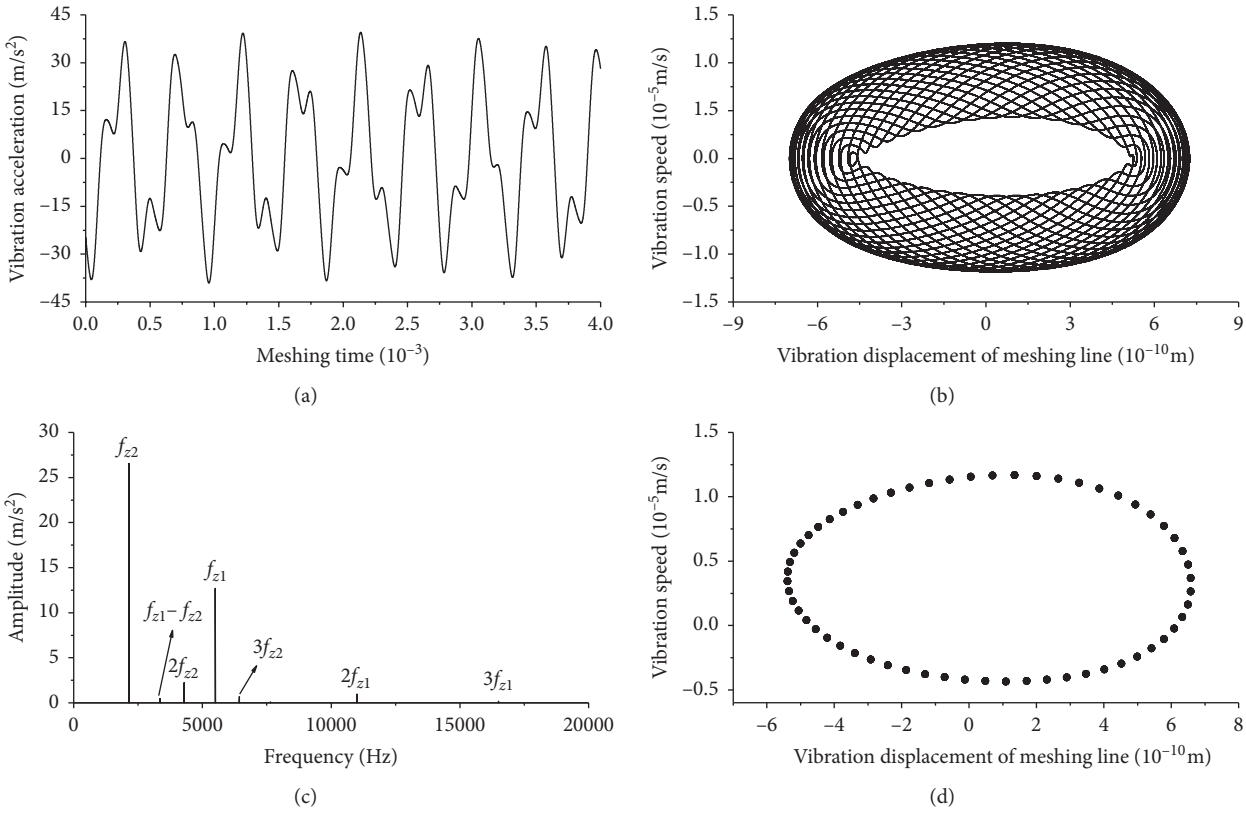

Figure 14: Vibration response of the output-stage gear pair of a two-stage helical gear transmission system at 15,000 rpm: (a) time-domain diagram, (b) phase diagram, (c) frequency-domain diagram, and (d) Poincaré section.

This phenomenon indicates that the vibrations of the two gear pairs in the two-stage helical gear transmission system affect each other, which makes the vibration of the system complicated. This is because the two-stage helical gear transmission system can be regarded as a multifrequency excitation system. In addition to the excitation frequency generated by its own, the vibration frequencies generated by the input-stage gear pair also have an excitation effect on the output-stage gear pair. At this time, the response frequency of system vibration is overlapping and a combination of the two gear pairs meshing frequency and its multiple frequencies. Due to the fact that the input-stage gear pair is the power source of the output-stage gear pair, the influence of the input-stage gear pair on the output-stage gear pair is

more obvious. This phenomenon is a prominent feature of the vibration response of two-stage helical gear transmission systems. Therefore, the response of system vibration becomes more complicated and the system's aperiodicity is enhanced.

5.2. Excitation of Meshing Impact. When substituting the meshing impact obtained above into the dynamic equations, the vibration response of the single-stage gear system is obtained under the input torques of 80 N · m, 100 N · m, and 120 N · m. The vibration acceleration diagram is shown in Figure 15.

Figure 15 is a vibration acceleration diagram of three different loads under the excitation of meshing impact. It shows that the vibration of the gear increases with the increase of the load. The 2nd- and 3rd-order superharmonic resonance occur when the rotating speed approaches 1/2 and 1/3 its resonance speed N_0. The RMS value of the vibration acceleration is significantly increased with the increase of the rotating speed excluding the resonance peak. The influence of rotating speed increasing on the system vibration is significantly far away from the resonance speed. This is because the meshing impact force increases with the increase of rotating speed, and the growth trend is approximately a linear relation. This is consistent with the conclusion in a previous literature that the dynamic load coefficient K_v increases with the increase of line speed [25].

To analyze the time domain characteristics of the helical gear system under the excitation of meshing impact, the time domain diagrams of the single-stage helical gear system at two different rotation speeds are shown in Figures 16 and 17.

In Figure 16, the main manifestation of the meshing impact zone is the abrupt change in the negative direction of vibration acceleration. It is because the rotating speed of the driven wheel will jump sharply when the meshing impact occurs, and the vibration acceleration of line of action will decrease sharply, combining with equation (23). In Figure 16, the vibration acceleration of the system is gradually attenuated by T_d, and $1/T_d$ is the natural frequency of the system. The meshing period T_z decreases gradually with the increase of rotational speed. The system will resonate when the meshing period T_z equals the vibration acceleration attenuation period T_d.

Figure 17 shows a time domain diagram of single-stage helical gear transmission system at 8,900 rpm under the excitation of meshing impact, where 8,900 rpm is the resonance speed of the single-stage helical gear transmission system.

Figure 17 clearly shows that the next impact is entered about one period of T_d after the previous impact, which is consistent with the conclusion above.

For further comparison of the dynamic characteristics of two-stage and single-stage helical gear transmission systems, the time domain diagrams of the input-stage gear pair and the output-stage gear pair are analyzed under the excitation of meshing impact at 3,000 rpm and 15,000 rpm, as shown in Figures 18 and 19.

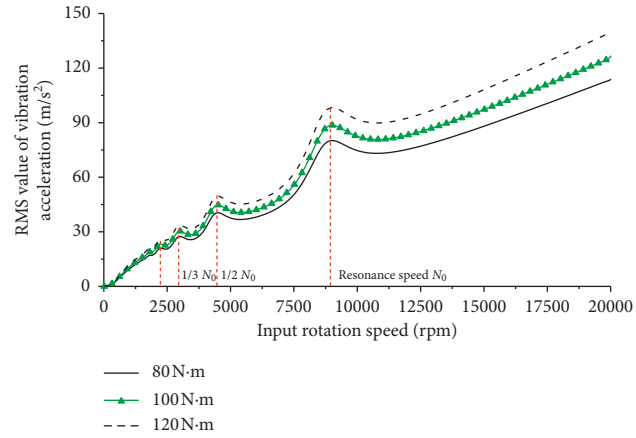

Figure 15: The vibration acceleration diagram under excitation of meshing impact of the single-stage gear system.

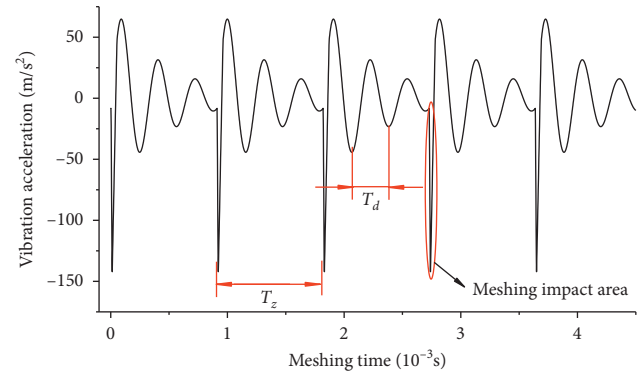

Figure 16: Time domain diagram of single-stage helical gear transmission under excitation of meshing impact at 3,000 rpm.

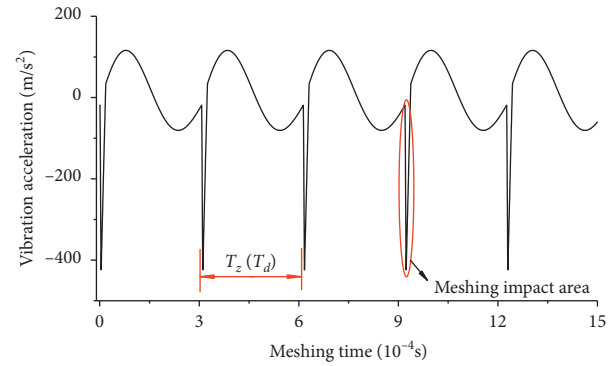

Figure 17: Time domain diagram of single-stage helical gear transmission under excitation of meshing impact at 8,900 rpm.

As can be seen in Figure 18(a), the two-stage helical gear transmission system under the excitation of meshing impact shows an abrupt change of vibration acceleration, which is consistent with the result in Figure 16. In addition to the abrupt change of vibration acceleration caused by its impact force, the output-stage gear pair has an abrupt change at the meshing impact positions corresponding to the input-stage gear pair. This is due to the influence of the input-stage gear pair on the output-stage gear pair. Because of the opposite

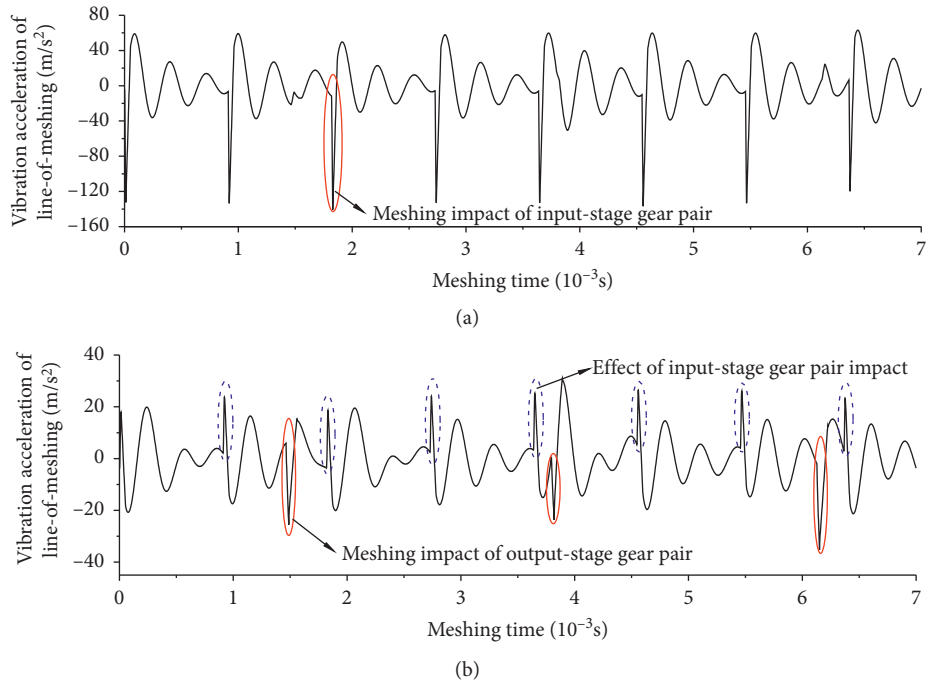

Figure 18: Time-domain diagram of two-stage helical gear transmission under excitation of meshing impact at 3,000 rpm, (a) the input-stage gear pair, (b) the output-stage gear pair.

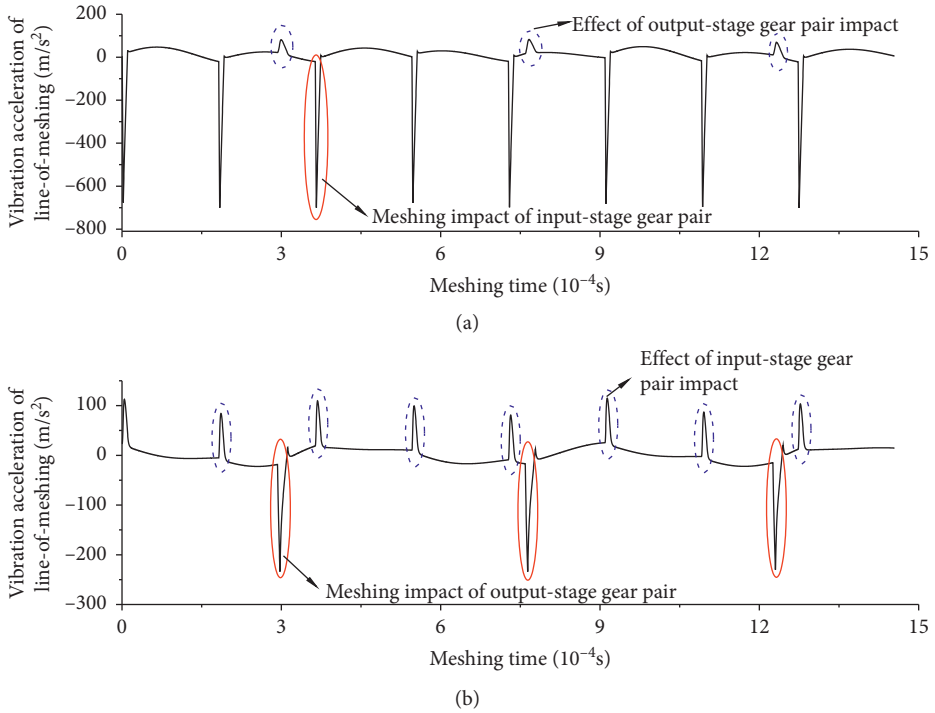

Figure 19: Time-domain diagram of two-stage helical gear transmission under excitation of meshing impact at 15,000 rpm, (a) the input-stage gear pair, (b) the output-stage gear pair.

rotational speeds of the two gear pairs, the directions of the acceleration abrupt change are opposite. In addition, the effect of the output-stage gear pair on the input-stage gear pair is not obvious as shown in Figure 18.

Figure 19 shows that, at the meshing time corresponding to the meshing impact of the input-stage gear pair, the output-stage gear pair has an obvious abrupt change of vibration acceleration, which is also consistent with the

analysis in Figure 16. The difference is that the influence of the meshing impact of the output-stage gear pair on the input-stage gear pair appears in Figure 19. As can be seen in Figure 19, the influence of the input-stage gear pair on the output-stage gear pair is significantly greater; this is mainly because the input-stage gear pair is the power source of the output-stage gear pair, and the input-stage gear pair has a relatively high rotation speed. Furthermore, the higher the input rotation speed is, the more obvious the interaction between the two gear pairs will be.

5.3. Excitation of Both. Substituting the TVMS and meshing impact obtained above into the dynamic equations simultaneously, the vibration responses of the single-stage gear system are obtained under three input conditions of 80 N · m, 100 N · m, and 120 N · m. The vibration acceleration diagram is shown in Figure 20.

Figure 20 is a vibration acceleration diagram of the comprehensive excitation under three kinds of loads. As can be seen, the vibration of the gear increases with the increase of the load. And 2nd- and 3rd-order superharmonic resonance occur when the rotating speed approaches 1/2 or 1/3 its resonance speed N_0; and the RMS value of the vibration acceleration is significantly increased with the increase of the rotational speed excluding the resonance peak. However, the tendency of the increase is slower than under the excitation of meshing impact. This is due to the slight decrease in system vibration with the increase of the rotation speed under the excitation of TVMS in the high-speed off-resonance region.

The vibration acceleration diagrams of the single-stage helical gear transmission system under three different excitations with the input torque of 100 N · m are compared in Figure 21. The system vibration under the excitation of meshing impact is larger than that under the excitation of TVMS. With the increase of the rotating speed, the system vibration under the excitation of meshing impact tends to be consistent with the excitation of both in the off-resonance zone. That is, the meshing impact is the main excitation component at high speed.

To compare the system responses under the three excitation modes, the diagrams of the frequency domain under three kinds of excitations for single-stage helical gear system at 12,000 rpm are shown in Figure 22, while under the excitation of TVMS independent, the third harmonic frequency is attenuated to zero. When the impact excitation component exists, the twentieth harmonic frequency still has a certain amplitude and its attenuation is slow. It is because the excitation frequency of the meshing impact is complicated; the system generates a lot of high-frequency harmonics. That is, the presence of the excitation of meshing impact makes the system vibration more complicated. This phenomenon is more prominent in the situation of high rotation speed. Therefore, more attention should be paid to the impact component in the optimization of vibration in the high-speed gear system.

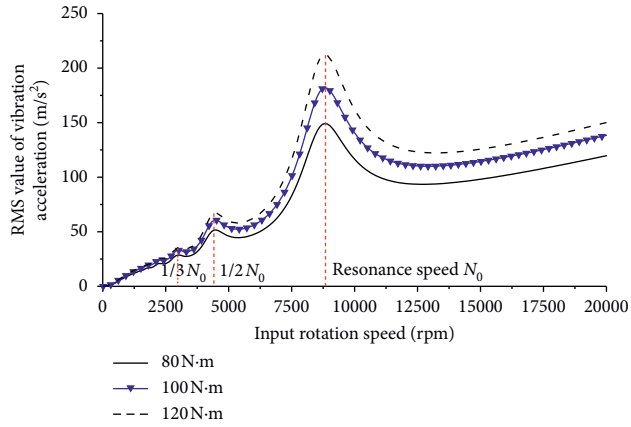

Figure 20: The vibration acceleration diagram under excitation of both for single-stage gear transmission system.

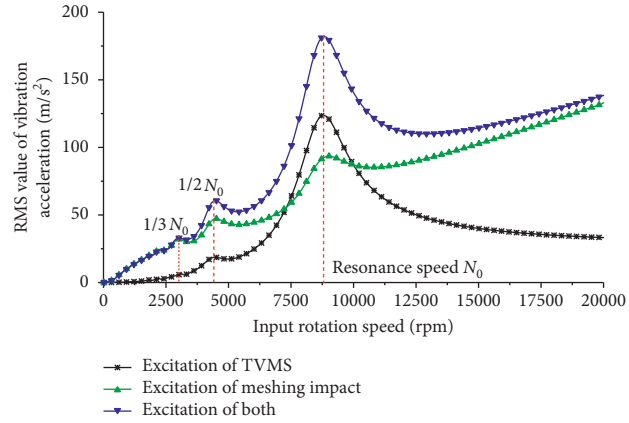

Figure 21: Vibration acceleration diagram for single-stage helical gear transmission system.

6. Effect of Tooth Surface Modification

Tooth surface modification is one of the commonly used methods to reduce vibration and noise in gear transmission. After proper modification of the gear, the meshing performance of the gear system can be effectively improved, the vibration and noise of the system can be reduced, and the service life of the gear system can be improved.

To analyze the effects of the two modification schemes, modification of the input-stage pinion and of the output-stage pinion, on the vibration reduction of the PEV high-speed two-stage helical gear transmission, the dynamic model is established by Romax software and shown in Figure 23, and the corresponding tooth surface modifications of the pinions are shown in Figures 24 and 25.

Then, the LTE curves of the two gear pairs, with and without modification, are simulated by Romax software, as shown in Figures 26 and 27.

In Figure 26, the peak-to-peak value of the LTE is reduced from 1.47 to 0.75, which is reduced by 49% after the modification of the input-stage pinion, while in Figure 27, the peak-to-peak value of the LTE is reduced from 0.95 to

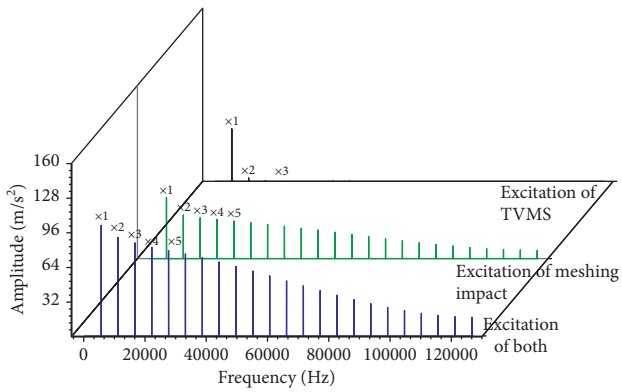

Figure 22: Frequency-domain diagram of single-stage helical gear transmission system at 12,000 rpm.

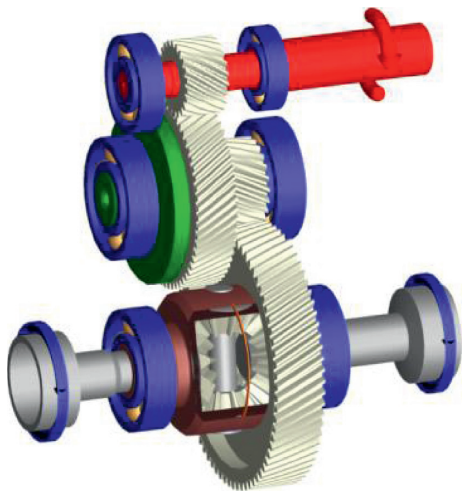

Figure 23: Model of the PEV reducer.

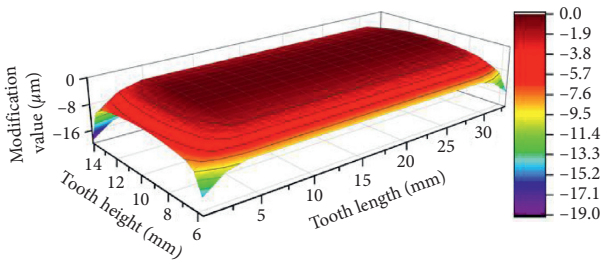

Figure 24: Modification of the input-stage pinion.

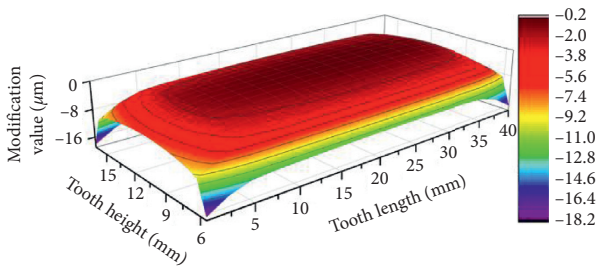

Figure 25: Modification of the output-stage pinion.

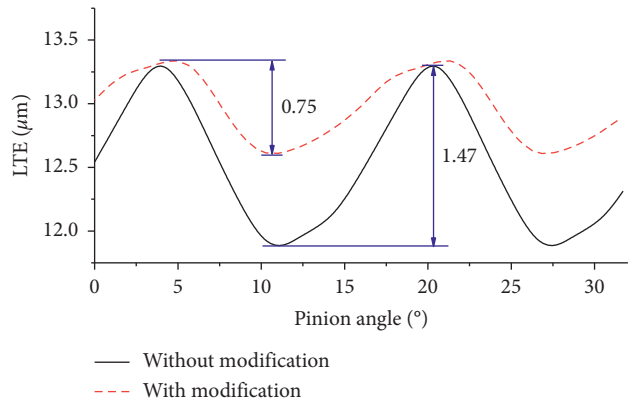

Figure 26: LTE of input-stage gear pair with and without modification.

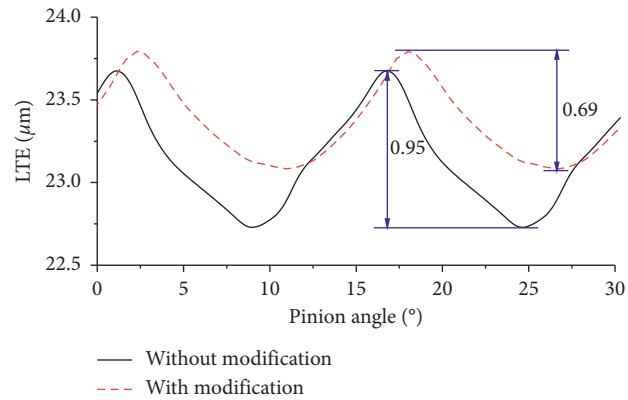

Figure 27: LTE of output-stage gear pair with and without modification.

0.69, which is reduced by 27.4% after the modification of the output-stage pinion.

To analyze the vibration reduction, the TVMS curves of two gear pairs are calculated based on LTEs. The TVMS curves are then substituted into the dynamic equations (3), and the system response is compared and analyzed after solving the equation. Figures 28 and 29 show the time domain responses at input speed 12,000 rpm under two kinds of modification schemes, separately.

Figure 28 shows the vibration response under the modification of the input-stage pinion. As can be seen from Figure 28(a), the fluctuation of the vibration acceleration in the input-stage gear pair is reduced, and the abrupt change of the vibration acceleration caused by the impact force is also greatly reduced. In Figure 28(b), the fluctuation of the vibration acceleration of the output-stage gear pair is reduced, and the abrupt change of the vibration acceleration caused by the impact of the input-stage gear pair is also reduced to a certain extent. However, the abrupt change of the acceleration caused by its impact force is not changed obviously.

As can be seen from Figure 29, after the modification of the output-stage pinion, the abrupt change of the vibration acceleration caused by the meshing impact of the output-

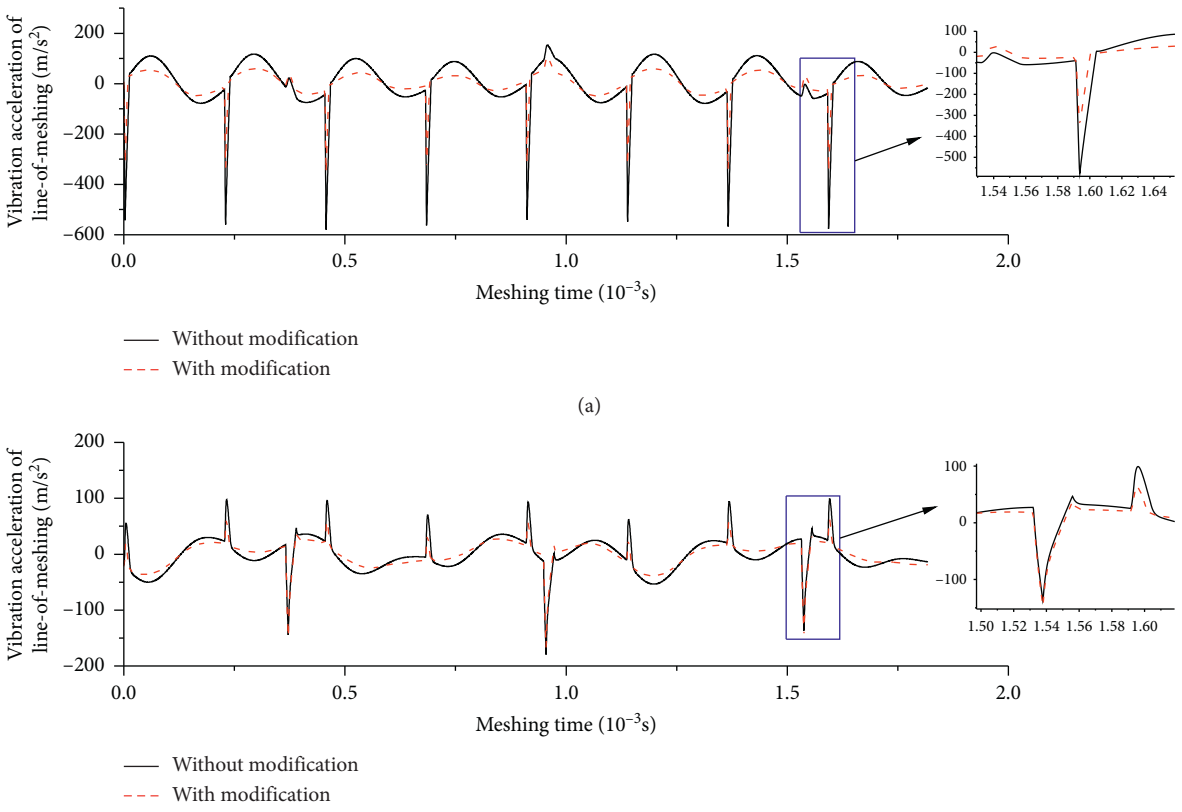

Figure 28: System vibration time domain at 12,000 rpm with the modification of the input-stage pinion: (a) time-domain diagram of input-stage gear pair and (b) time-domain diagram of output-stage gear pair.

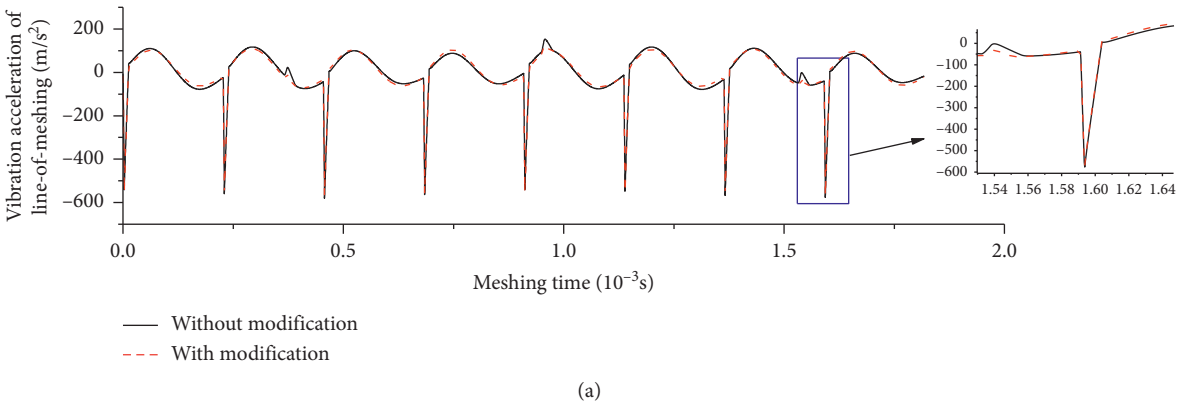

Figure 29: Continued.

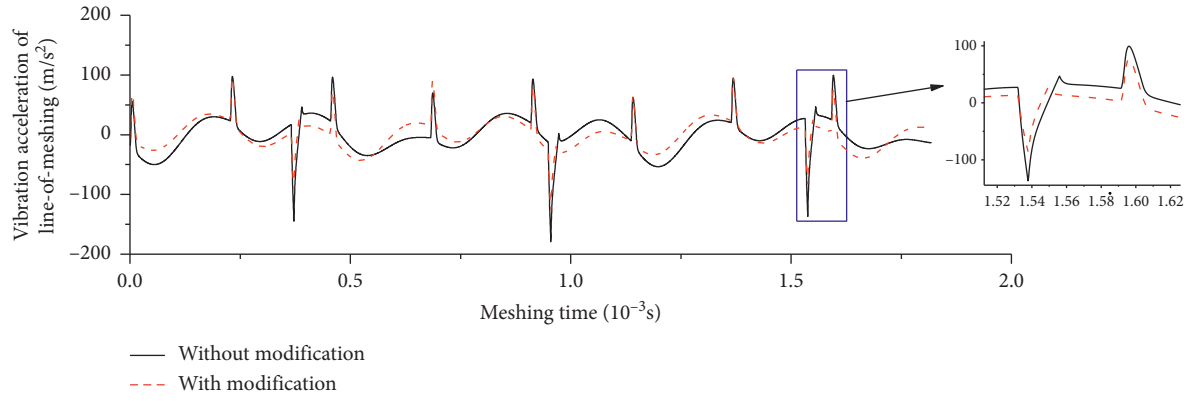

(b)

Figure 29: System vibration time domain at 12,000 rpm with the modification of the output-stage pinion: (a) time-domain diagram of input-stage gear pair and (b) time-domain diagram of output-stage gear pair.

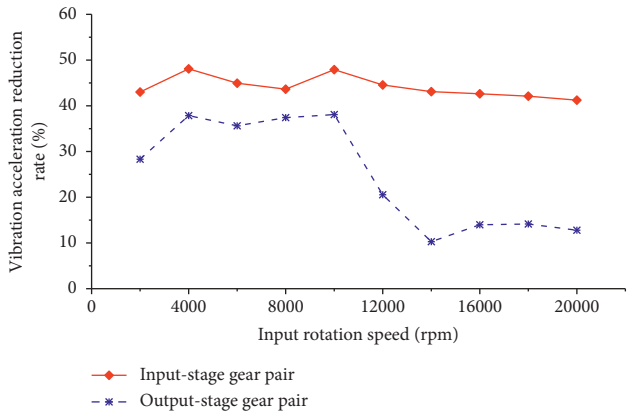

Figure 30: Vibration reduction effect of the system with the modification of input-stage pinion.

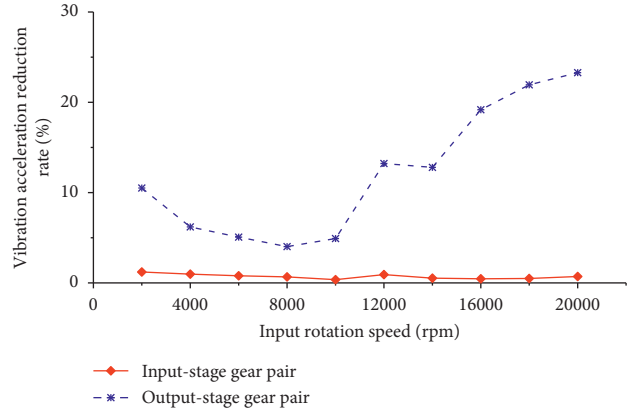

Figure 31: Vibration reduction effect of the system with the modification of output-stage pinion.

stage gear pair is reduced. However, the vibration acceleration of the input-stage gear pair is not significantly changed.

The phenomena in Figures 28 and 29 coincide with the results of the previous analysis that the vibration between the input-stage gear pair and the output-stage gear pair affects each other, and the influence of the former on the latter is obviously greater than that of the latter on the former.

To compare the effect of vibration reduction under the two kinds of modifications, the dynamic equations are solved, and the RMS values of the vibration acceleration are calculated at various input rotation speeds, as shown in Figures 30 and 31, where the vibration acceleration reduction rate represents the percentage reduction of RMS value of vibration acceleration on each stage before and after modification.

Figure 30 shows that, after modification of the input-stage pinion, not only does the input-stage gear pair have a damping effect (41.2%~48.1%), but also the vibration of the output-stage gear pair is significantly reduced (10.3%~37.8%). Figure 31 shows that, after modification of the output-stage pinion, the vibration of the output-stage gear pair is significantly reduced (4.2%~23.3%), but the vibration of the reduction of the input-stage gear pair is not significant (0.3%~1.2%).

According to the analysis of the system dynamic characteristics in the previous section, the phenomena in Figures 30 and 31 are due to the fact that the vibration of the input-stage gear pair has a great influence on the output-stage gear pair. Thus, the modification of the input-stage pinion will significantly weaken the vibration on both stages. Therefore, more attention should be paid to the input-stage gear pair in the modification design of multistage gear transmission.

7. Conclusions

The RMS value of the vibration acceleration is not significantly increased with the increase of the rotating speed excluding the resonance region under the excitation of TVMS. The influence of rotating speed increasing on vibration is not significantly away from the resonance speed. The RMS value of the vibration acceleration is significantly increased with the increase of the rotating speed under the excitation of meshing impact and the excitation of both. However, the increasing tendency of the vibration

acceleration under the excitation of both is slower than that of under the excitation of meshing impact.

In the high-speed off-resonance region, the influence of meshing impact on the system vibration is greater than TVMS. That is, the meshing impact becomes the main excitation component at high speed.

The vibration of the two gear pairs has a mutual effect in the two-stage gear transmission. The main manifestation is that the vibration response frequency of one gear pair contains not only its own meshing frequency, but also the coupling frequencies. This phenomenon makes the vibration response of the high-speed gear transmission system more complicated.

Modification of the input-stage pinion will lead to significant vibration reduction for both stages in the two-stage high-speed helical gear transmission, about 41.2%~48.1% reduction for the input-stage and 10.3%~37.8% for the output-stage, while it only has a limited effect on its own stage when the output-stage pinion is modified, about 4.2%~23.3% reduction for output-stage but only 0.3%~1.2% for the input-stage. Therefore, more attention should be paid to the input-stage gear pair in the modification design of multi-stage gear transmissions.

Data Availability

The data used to support the conclusions of this study are included within the article.

Conflicts of Interest

The authors declare that they have no conflicts of interest.

Acknowledgments

The authors would like to acknowledge the financial aid and support from the Key Laboratory of Shaanxi Province for Development and Application of New Transportation Energy (Chang'an University) Open Foundation (grant no. 300102220507), the National Natural Science Foundation of China (grant nos. 51705419 and 61701397), the China Postdoctoral Science Foundation (grant no. 2019M653702), the Postdoctoral Research Project of Shaanxi Province (grant no. 2018BSHEDZZ10), and the Shaanxi Provincial Department of Education Service Local Special (Industrialization) Plan Project (19JC030).

References

[1] F. H. Gandoman, A. Ahmadi, P. V. D. Bossche et al., "Status and future perspectives of reliability assessment for electric vehicles," *Reliability Engineering & System Safety*, vol. 183, pp. 1–16, 2019.

[2] P. Walker, B. Zhu, and N. Zhang, "Powertrain dynamics and control of a two speed dual clutch transmission for electric vehicles," *Mechanical Systems and Signal Processing*, vol. 85, pp. 1–15, 2017.

[3] M. M. F. Sabri, K. A. Danapalasingam, and M. F. Rahmat, "A review on hybrid electric vehicles architecture and energy management strategies," *Renewable and Sustainable Energy Reviews*, vol. 53, pp. 1433–1442, 2016.

[4] K. C. Bayindir, M. A. Gozukucuk, and A. Teke, "A comprehensive overview of hybrid electric vehicle: powertrain configurations, powertrain control techniques and electronic control units," *Energy Conversion and Management*, vol. 52, no. 2, pp. 1305–1313, 2011.

[5] M. G. Tehrani, J. Kelkka, J. Sopanen et al., "Transmission configuration effect on total efficiency of electric vehicle power train," in *Proceedings of the 2014 16th European Conference on Power Electronics and Applications 2014*, Lappeenranta, Finland, August 2014.

[6] C. G. Cooley and R. G. Parker, "A review of planetary and epicyclic gear dynamics and vibrations research," *Applied Mechanics Reviews*, vol. 66, no. 4, Article ID 040804, 2014.

[7] H. Yonezawa, I. Kajiwara, C. Nishidome et al., "Vibration control of automotive drive system with backlash considering control period constraint," *Journal of Advanced Mechanical Design, Systems, and Manufacturing*, vol. 13, no. 1, pp. 1–16, 2019.

[8] X. Liu, Z. Wu, J. Lu et al., "Investigation of the effect of rotation speed on the torsional vibration of transmission system," *Journal of Advanced Mechanical Design, Systems, and Manufacturing*, vol. 13, no. 4, pp. 1–12, 2019.

[9] A. Mbarek, A. Hammami, A. Fernandez Del Rincon, F. Chaari, F. Viadero Rueda, and M. Haddar, "Effect of load and meshing stiffness variation on modal properties of planetary gear," *Applied Acoustics*, vol. 147, pp. 32–43, 2019.

[10] A. Fernández, M. Iglesias, A. De-Juan, P. García, R. Sancibrián, and F. Viadero, "Gear transmission dynamic: effects of tooth profile deviations and support flexibility," *Applied Acoustics*, vol. 77, pp. 138–149, 2014.

[11] J.-L. Dion, S. Le Moyne, G. Chevallier, and H. Sebbah, "Gear impacts and idle gear noise: experimental study and nonlinear dynamic model," *Mechanical Systems and Signal Processing*, vol. 23, no. 8, pp. 2608–2628, 2009.

[12] M.-L. Sun, C.-H. Lu, Z.-E. Liu, Y. Sun, H. Chen, and C. Shen, "Classifying, predicting, and reducing strategies of the mesh excitations of gear whine noise: a survey," *Shock and Vibration*, vol. 2020, Article ID 9834939, 20 pages, 2020.

[13] C.-S. Song, S.-W. Zhou, C.-C. Zhu et al., "Modeling and analysis of mesh stiffness for straight beveloid gear with parallel axes based on potential energy method," *Journal of Advanced Mechanical Design, Systems, and Manufacturing*, vol. 12, no. 7, pp. 1–14, 2018.

[14] A. Saxena, A. Parey, and M. Chouksey, "Effect of shaft misalignment and friction force on time varying mesh stiffness of spur gear pair," *Engineering Failure Analysis*, vol. 49, pp. 79–91, 2015.

[15] M.-H. Yin, G.-D. Chen, and H. Su, "Theoretical and experimental studies on dynamics of double-helical gear system supported by journal bearings," *Advances in Mechanical Engineering*, vol. 8, no. 5, pp. 1–13, 2016.

[16] X. Tang, L. Zou, W. Yang, Y. Huang, and H. Wang, "Novel mathematical modelling methods of comprehensive mesh stiffness for spur and helical gears," *Applied Mathematical Modelling*, vol. 64, pp. 524–540, 2018.

[17] L. Han and H. Qi, "Influences of tooth spalling or local breakage on time-varying mesh stiffness of helical gears," *Engineering Failure Analysis*, vol. 79, pp. 75–88, 2017.

[18] M. B. Sánchez, M. Pleguezuelos, and J. I. Pedrero, "Approximate equations for the meshing stiffness and the load sharing ratio of spur gears including hertzian effects," *Mechanism and Machine Theory*, vol. 109, pp. 231–249, 2017.

[19] Y. Chen, M. Ahmat, and Z.-T. Huo, "Dynamic meshing incentive analysis for wind turbine planetary gear system,"

Industrial Lubrication and Tribology, vol. 69, no. 2, pp. 306–311, 2017.

[20] F. Wang, X. Xu, and Z.-D. Fang, "New method with experimental validation for power transmission process analysis on herringbone gear train system," *International Journal of Acoustics and Vibration*, vol. 22, no. 4, pp. 519–535, 2017.

[21] C. Zhou and S. Chen, "Modeling and calculation of impact friction caused by corner contact in gear transmission," *Chinese Journal of Mechanical Engineering*, vol. 27, no. 5, pp. 958–964, 2014.

[22] J.-F. Du, *Tooth Contact Pattern Analysis and Design Technology Research of Cycloid Hypoid Gears*, pp. 53–57, Northwestern Polytechnical University, Xi'an, China, 2015.

[23] Z.-D. Fang, "Loaded tooth contact analysis of modified helical gears," *Journal of Aerospace Power*, vol. 12, no. 3, pp. 251–254, 1997, in Chinese.

[24] Editorial Board of Gear Manual, *Gear Manual*p. 101, 2th edition, China Machine Press, Beijing, China, 2000.

[25] R.-F. Li and J.-J. Wang, *Gear System Dynamics*, pp. 412-413, Science Press, Beijing, China, 1997.